

NJC

New Journal of Chemistry

Accepted Manuscript

A journal for new directions in chemistry

This article can be cited before page numbers have been issued, to do this please use: J. T. Bhanushali, D. Prasad, K. N. Patil, G. V. Ramesh Babu, I. Kainthla, S. R. R. Kamaraju, A. H. Jadhav and B. M. Nagaraja, *New J. Chem.*, 2019, DOI: 10.1039/C9NJ03067K.



This is an Accepted Manuscript, which has been through the Royal Society of Chemistry peer review process and has been accepted for publication.

Accepted Manuscripts are published online shortly after acceptance, before technical editing, formatting and proof reading. Using this free service, authors can make their results available to the community, in citable form, before we publish the edited article. We will replace this Accepted Manuscript with the edited and formatted Advance Article as soon as it is available.

You can find more information about Accepted Manuscripts in the [Information for Authors](#).

Please note that technical editing may introduce minor changes to the text and/or graphics, which may alter content. The journal's standard [Terms & Conditions](#) and the [Ethical guidelines](#) still apply. In no event shall the Royal Society of Chemistry be held responsible for any errors or omissions in this Accepted Manuscript or any consequences arising from the use of any information it contains.

ARTICLE

Selectively regulated vapour phase dehydrogenation of 1,4-butanediol to γ -butyrolactone employing a copper based ceria catalyst

Received 00th January 20xx,
Accepted 00th January 20xx

DOI: 10.1039/x0xx00000x

Jayesh T. Bhanushali^a, Divya Prasad^a, Komal N. Patil^a, Gurram Venkata Ramesh Babu^b, Itika Kainthla^a, Kamaraju Seetha Rama Rao^b, Arvind H. Jadhav^{a,*}, Bhari Mallanna Nagaraja^{a,*}

The growing pursuit for the viable application of γ -butyrolactone (GBL) as an industrially important product offers probabilities to use 1,4-butanediol (1,4-BDO) as a potential reactant. In this regard different proportions of copper based ceria catalysts (5, 10, 15, 20CC) were synthesized using wet impregnation method and its catalytic activity was tested for vapour phase dehydrogenation of 1,4-BDO to GBL at temperatures from 240-300 °C. The synthesized copper based ceria catalysts (5CC, 10CC, 15CC, 20CC) were characterized by various analytical tools and their consequent results revealed that the activity of CC catalysts was influenced by the physicochemical properties of materials. In order to determine the influence of various supports on the catalytic activity, addition of 10 wt.% copper (Cu) on TiO₂, Al₂O₃, ZnO, ZSM-5, SBA-15 supports was carried out and their respective influence on the catalytic activity was also experimentally established. The most outstanding catalytic activity was seen for the 10 wt.% copper based ceria catalyst with a high conversion of 93% and selectivity of 98% at 240 °C. The factors like high surface area, better dispersion and basicity of the active sites had a marked impact on the catalytic activity. Mechanistic aspects suggested that 1,4-BDO undergoes dehydrogenation over copper surface to give 4 hydroxybutanal followed by hemiacetylation and subsequent dehydrogenation to give GBL as the selective product. In terms of stability of catalysts, the time on stream for 10 wt.% copper based ceria catalyst maintained a stable GBL selectivity of 98% for upto 7 h.

Keywords: Dehydrogenation, Copper-ceria catalyst, 1,4-butanediol, gamma butyrolactone

Introduction

Oxidation of alcohols is a widely studied area in the field of research. However, selective oxidation of alcohols not only needs explicit oxidants and extreme reaction conditions but also generates a huge amount of waste which is not in accordance with the laws of green chemistry. Vapour phase reaction is advantageous considering the fact that these are solvent free reactions and the resultant products deliver negligible impurities. Dehydrogenation of 1,4-butanediol (1,4-BDO) is a prime reaction as it generates γ -butyrolactone (GBL), which is the main precursor for synthesis of N-methyl-2-pyrrolidone, 2-pyrrolidone, N-vinyl-2-pyrrolidone, polyvinylpyrrolidone, herbicides and rubber additives¹. It can also be considered as a prospective replacement for many

chlorinated solvents which come across as potential environmental threats². Extensive efforts have been put in the synthesis of GBL via dehydrogenation and lactonization of 1,4-BDO due to its outstanding nature as a reactant. Conventional synthesis of GBL can be done employing two methods which include (i) hydrogenation of maleic anhydride (MA) and (ii) dehydrogenation of 1,4-BDO. The former method has been extensively used owing to the less cost of MA but the process is disadvantageous because synthesis of MA emits CO₂ which is a greenhouse gas produced during oxidation of benzene and n-butane. The latter process is economical as 1,4-BDO is commercially manufactured by hydrogenation of acetylene and formaldehyde also popularly known as Reppe process^{2,3}. However, acetylene is generated from fossil fuels and is an expensive raw material. Therefore, researchers have developed an alternative route for the synthesis of 1,4-BDO using renewable biomass like glucose, thereby making it an economical and environmentally benign process^{2,4}. Additionally, two molecules of hydrogen which are generated on dehydrogenative cyclization of 1,4-BDO can be used as a source of fuel. Various catalysts have been employed in synthesis of GBL which includes transition metal based

^aCentre for Nano and Material Sciences, Jain University, Jain Global Campus, Kanakapura, Ramanagaram, Bangalore 562112, Karnataka, India

E-mail: j.arvind@jainuniversity.ac.in, bm.nagaraja@jainuniversity.ac.in;

Fax: +91-80-2757-7211; Tel: +91-80-2757-7212

^bCatalysis & Fine Chemicals Division, CSIR-Indian Institute of Chemical Technology, Hyderabad 500007, Telangana, India

catalysts such as Cu/ZnO/Al₂O₃¹, Cu-ZnO-ZrO₂-Al₂O₃³, Cu/MgO⁵, Cu-Cr-Mn⁶, Cu-CaO-Na₂O/SiO₂⁷, as well as noble metal based catalysts such as Au/TiO₂⁸ and Au/Fe₂O₃⁹. These catalysts are however not very cost effective and are not abundantly available for usage, thereby paving way for synthesis and implementation of economical catalysts.

On the other hand, supports play an active role in the selective synthesis of GBL. Acidic supports like Al₂O₃, Al₂O₃-SiO₂, WO₃ based catalysts, metal oxide based Ru catalysts generate tetrahydrofuran (THF) as the selective product via dehydration pathway whereas copper based catalysts with basic supports (MgO, ZnO) have been reported to selectively form GBL¹⁰. In addition, the degree of dispersion of active components within the catalyst system regulates its catalytic performance. Higher dispersion can pilot better catalytic activity which can be achieved by selecting a feasible support satisfying the primary requirement of a non-reactive active part of the catalyst and secondary requirement of high surface area. The reaction thermodynamics and kinetic factor depends on the metal support interaction of the catalyst which indirectly governs its catalytic activity. Ceria as a support has been used for various reactions such as oxidation of soot¹¹, water gas shift reaction¹², reduction of NO with NH₃¹³, synthesis of cyclic carbonates using glycol and CO₂¹⁴ and oxy-dehydrogenation of ethane¹⁵. The selection of ceria as a support is convinced by the tunability of its textural properties which is optimistic for the reaction and also because of its interaction with different metals¹³. Supportingly, copper has been used in various reactions as an active metal due to its easily tunable surface area, variation in particle size and dispersive nature¹⁶. Copper based catalysts have also been notably used in varied research areas like combustion of styrene¹⁷, oxidation of benzyl alcohol¹⁸, oxidation of butanol¹⁹ and hydrogenation of benzaldehyde²⁰.

Herein, we report for the first time the utilization of copper based ceria catalysts (5CC, 10CC, 15CC, 20CC) for dehydrogenation of 1,4-BDO to GBL under vapour phase conditions with variation in copper loading. The different copper based ceria catalyst have been prepared by wet impregnation method and subsequently tested for dehydrogenation of 1,4-BDO to GBL by varying the reaction temperatures and metal loading on ceria support. The stability of the catalyst with time on stream has also been analysed. Additionally, a comparison has been done with copper supported over various supports like SBA-15, ZnO, TiO₂, ZSM-5, Al₂O₃ in order to determine the influence of copper addition on these supports on the catalytic activity. Also, a brief summary of already reported catalysts has been shown in order to point out the versatility of the present work. A probable mechanism as reported in literature has also been illustrated for the selective dehydrogenation of 1,4-BDO to GBL.

Experimental

Materials:

Copper nitrate trihydrate (Cu(NO₃)₂·3H₂O) (M/s. Sigma Aldrich, USA), Ammonium ceric nitrate (NH₄)₂[Ce(NO₃)₆]·6H₂O, Zinc nitrate hexahydrate (Zn(NO₃)₂·6H₂O) (M/s. S.D. Fine Chemicals, India), were purchased and used without further purification. γ-Al₂O₃, TiO₂ and HZSM-5 were commercially purchased and used as received. SBA-15 was synthesized following synthetic procedure published elsewhere^{21, 22}. Deionized water was used for the synthesis of all the catalysts.

Preparation of Cu/CeO₂ (CC):

Different copper based ceria catalysts with variation in copper loading (5, 10, 15 and 20 wt.%) were synthesized using the traditional wet impregnation method. The required amount of copper nitrate trihydrate (Cu(NO₃)₂·3H₂O) was added into a pre-mixed solution of ammonium ceric nitrate (NH₄)₂[Ce(NO₃)₆] and water. Further, the solution was heated to 65 °C with constant stirring in order to evaporate excess water. The resultant fine powder was subjected to drying at 100 °C for 12 h in an oven and finally calcined in static air flow at 450 °C for 4 h with a ramping rate of 3 °C min⁻¹. Catalysts thus obtained were designated as 5CC, 10CC, 15CC and 20CC for 5, 10, 15 and 20 wt.% of copper loadings respectively and were subsequently characterized using various analytical tools. Similar procedure was followed for the synthesis of copper catalysts on TiO₂, Al₂O₃, ZnO, ZSM-5, SBA-15 support matrices.

Characterization:

Powder X-ray diffraction patterns of the catalysts were recorded on a Ultima-IV X-ray diffractometer (M/s. Rigaku Corporation, Japan) using Ni filtered Cu Kα radiation (λ = 1.5406 Å) with rate of 2° min⁻¹ and a 2θ scan range of 10-80° at 40 kV and 30 mA. Crystalline phases were identified by comparison with the reference data from international centre for diffraction data (ICDD) files.

Surface area and pore size distribution analysis were conducted with N₂ at liquid N₂ temperature (-196 °C) on a Belsorp-Max (M/s. Microtrac BEL, Japan.) for getting the multipoint surface area using the Brunauer Emmett and Teller (BET) analysis method and total pore volume by Barrett-Joyner-Halenda (BJH) method. Prior to the measurement, the samples were degassed at 200 °C for 2 h in order to expel the inter layer moisture under vacuum control. Field emission scanning electron microscopy (FE-SEM) measurements were made using JEOL JSM-7100F, Singapore. Transmission Electron Microscopy was used to check the interior architecture, SAED pattern and lattice fringes of the material using TEM microscope (JEOL JEM-200CX). The accelerating voltage of the electron beam for the microscope was set for 200 kV.

The H₂-Temperature programmed reduction (TPR) analysis was carried out in an indigenous instrument consisting of quartz reactor attached to a six-port valve attached with a thermal conductivity detector (M/s Mayura Analyticals, India). Approximately 50 mg of the sample was loaded in the isothermal zone of a quartz reactor (i.d. = 6 mm, length = 300 mm) and subjected to pre-treatment at 300 °C for 1 h with the heating rate of 10 °C min⁻¹ in He flow to facilitate the desorption of physisorbed water. After degassing, the sample was cooled to 100 °C and the He gas was replaced with a reducing gas (5% H₂/Ar) with a flow rate of 30 mL min⁻¹. The temperature was linearly increased to 700 °C with a ramping rate of 10 °C min⁻¹ and maintained at the same temperature for 0.5 h. The

hydrogen consumption was monitored by standard GC software. The H₂ uptake values were calculated using standard reference value obtained by injecting known loop volume of H₂ using six-port valve.

Additionally, measurement of percentage of copper dispersion, metal surface area and metal particle size was carried out using N₂O chemisorption in the above mentioned instrument equipped with the Hayasep T column. In a typical analysis procedure, 100 mg of sample was loaded into quartz reactor and pre-treated at 300 °C for 1 h in He flow. Later the sample was reduced at its appropriate reduction temperature for 3 h in the presence of H₂ flow. Then the sample was cooled to room temperature and N₂O gas (5% N₂O/He) is injected in pulses till the attainment of the saturation point.

Similarly, measurement of acidity and basicity of the catalysts were carried out using NH₃ and CO₂ temperature programmed desorption (TPD) analysis in the above mentioned instrument. Prior to desorption, catalysts were pre-treated in He flow for 1 h at 300 °C and cooled down to 100 °C in the He environment. Subsequently, catalysts were saturated with 5% NH₃/He or 5% CO₂ at 100 °C for 0.5 h, followed by stripping with He for 0.5 h to remove the physisorbed NH₃ and CO₂ at the same temperature. Later, the temperature was raised from 100 to 700 °C with a ramping rate of 10 °C min⁻¹ and the desorbed gas was monitored with TCD.

The type of acidic and basic sites was determined using pyridine adsorbed ATR-IR and isopropanol adsorbed ATR-IR spectra on a Perkin Elmer ATR-IR instrument. In a typical experimental procedure, the catalyst was subjected to degassing under vacuum at 200 °C for 3 h followed by treatment with dry pyridine and isopropanol respectively. Later, the samples were heated at 120 °C for 1 h in order to remove excess pyridine and isopropanol. After cooling the samples to room temperature, ATR-IR spectra of respective-adsorbed samples were recorded. In order to quantify the deposition of coke on the catalyst surface thermogravimetric analysis was performed using a TA-Q500 series (M/s TA instruments, USA).

Catalytic reaction:

Catalytic activity studies were performed in a fixed bed down flow quartz reactor at atmospheric pressure. For a typical reaction, 0.5 g of catalyst was loaded in the reactor and subjected to reduction with H₂ for 3 h at 280 °C. The reaction was performed within the range of 240-300 °C using N₂ (30 mL min⁻¹) as an oxidant at atmospheric pressure. 1,4-BDO was introduced by a liquid feed pump (M/s. B. Braun, Germany) with a feed rate of 1 mL h⁻¹. The products were collected at regular intervals in an ice cold trap and analyzed on a flame ionization detector (FID) equipped gas chromatograph, GC-7820 A (M/s. Agilent, USA) using a capillary column HP-5, 19091J-413 (30 m length, 0.32 mm inner diameter and 0.25 μm film thickness).

The quantification of each component in the product mixture was done by injecting a known amount of authentic sample (1,4-BDO and GBL) and comparing the GC area of authentic sample with that of the product mixture. The percentage conversion of 1,4-BDO (C_{BDO}) and percentage selectivity of GBL (S_{GBL}) were calculated as: $C_{BDO} = (BDO_{in} - BDO_{out}) * 100 / BDO_{in}$; $S_{GBL} = Y_{GBL} * 100 / C_{BDO}$ where,

BDO_{in} is the amount of 1,4 BDO at inlet and BDO_{out} is the amount of 1,4-BDO present in product mixture and Y_{GBL} is the yield of GBL.

Results and Discussion

Structural and textural properties of catalysts

BET surface area and pore size distribution: The textural properties obtained for 5CC, 10CC, 15CC, 20CC catalysts are summarized in **Table 1** along with the respective nitrogen sorption curves as depicted in **Fig. 1**. The use of pristine ceria support without any copper adherence reveals Type-II isotherm (**Fig. 1(a)**). The addition of 5, 10, 15, 20 wt.% copper on ceria support shows Type-IV isotherm which is characteristic feature of mesoporous materials (**Fig. 1(b-e)**). This shows that introduction of copper metal on the ceria support is responsible for the mesoporous nature of the 5CC catalyst (**Fig. 1(b)**). This mesoporosity is retained on further loading of copper species in the 10CC, 15CC, 20CC catalysts which can be observed in the isotherms obtained (**Fig. 1(c-e)**). The steep curve observed in the adsorption isotherm corresponds to the capillary condensation of pores²³. Interestingly, there is decrease in the surface area for 5CC catalyst from 34 m² g⁻¹ to 14 m² g⁻¹. This shows that there is deposition of copper species onto the support matrix²⁴. Notably, on further increase in copper addition (10CC), the surface area increases to 34 m² g⁻¹ signifying that copper on ceria support (10CC) prevents sintering²⁵. With further addition of copper particles (15CC and 20CC), the surface area of the catalysts increases to 58 m² g⁻¹ and 74 m² g⁻¹, respectively. Additionally, the increment in surface area of 10CC, 15CC and 20CC catalysts can also be very well explained based on increase in pore volume and fine dispersion of copper particles on the ceria support²⁶. Also, the mesoporous nature of catalysts can be related to increase in porosity of catalysts (5CC, 10CC, 15CC and 20CC) which can be clearly seen to be in accordance with the increase in pore volume²⁶.

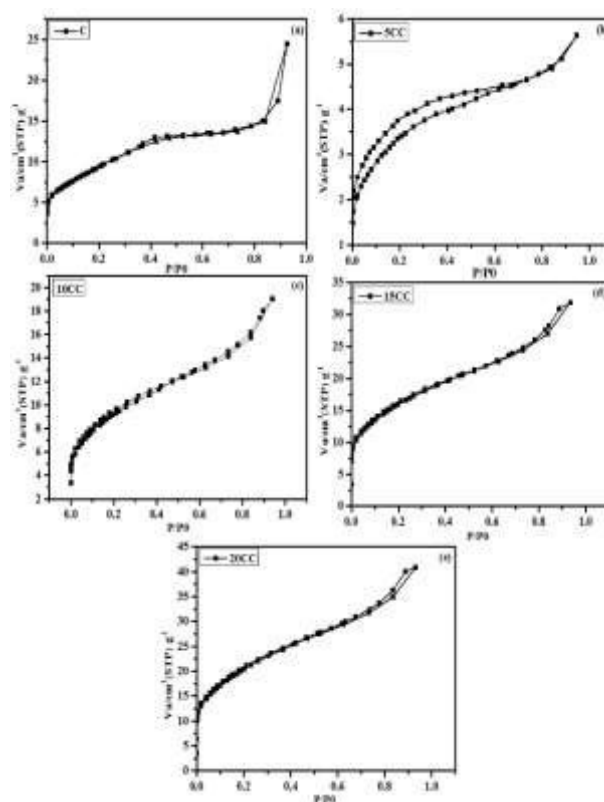


Fig. 1. N₂ sorption isotherms of Cu/CeO₂ catalysts.

The increase in surface area combined with the mesoporosity of the catalysts provide good adsorption sites for reactant molecules to gain access to these sites and resultantly leads to easy desorption of product molecules formed²⁷.

X-ray Diffraction studies: The X-ray diffraction analysis for pristine ceria support, calcined copper based ceria catalysts and reduced

copper based ceria catalysts was performed and the obtained data is displayed in **Fig. 2**. The diffractogram as shown in the **Fig. 2(a)** and **Fig. 2(b)** confirms the presence of ceria at 2θ values 28.47°, 32.98°, 47.60°, 56.44°, 59.25°, 69.95° and 77.45° in both calcined as well as reduced catalysts. It can also be confirmed that ceria particles in the

Table 1. Textural characteristics of Cu/CeO₂ catalysts with different metal loadings.

Sr. No.	Catalyst	Surface area (m ² g ⁻¹)	Pore volume (cm ³ g ⁻¹)	Pore diameter (nm)	Crystallite size (nm)	H ₂ uptake (mmol g ⁻¹)	Cu metal surface area (m ₂ g ⁻¹)	Cu particle size (nm)	Cu dispersion (%)
1	C	34	0.029	2.52	14.70	-	-	-	-
2	5CC	14	0.004	2.52	9.12	4.7	30	1.11	90
3	10CC	34	0.020	2.52	12.42	7.6	56	1.21	86
4	15CC	58	0.034	2.52	6.06	7.3	65	1.55	67
5	20CC	74	0.044	2.52	7.20	12.4	32	4.15	25

catalyst exist in cubic system [ICDD: 65-5923] along with hkl values of (111), (200), (220) and (311) in the crystal plane²⁷. Interestingly, the peaks corresponding to copper oxide (CuO) and copper are not observed upto 20 wt.% copper loading signifying that the copper species is highly dispersed in the catalyst system²⁴.

However, peaks corresponding to CuO at 2θ: 35.42°, 38.61°, 61.50° and 66.38° along with copper at 2θ: 43.35°, 49.85°, 77.68° are observed for both 20CC calcined and 20CC reduced catalysts, respectively. CuO particles in the calcined (20CC) catalyst system exist in monoclinic phase [ICDD: 2-1040] with hkl values (002), (111)²⁸ and copper particles present in the reduced (20CC) catalyst system exhibit cubic phase [ICDD: 3-1005] with hkl values (111)²⁹. Further, non-existence of CuO particles in the reduced (20CC) catalyst suggests that on reduction the CuO particles are completely diminished. Additionally, comparison of crystallite size suggests that addition of copper particles on the support matrix decreases the crystallite size. Hence, the decrease in crystallite size suggests that increase in copper loading increases the crystallinity of the catalyst system. This is due to the suppression in the growth of crystal which is attributable to the introduction of copper species into ceria support matrix²⁷. Surprisingly, 10CC catalyst unveils higher crystallite size (12.42 nm) when compared to 5CC (9.12 nm), 15CC (6.06 nm) and 20CC (7.20 nm) catalysts as displayed in **Table 1**.

H₂-temperature programmed reduction studies: The evaluation of reduction behaviour of copper based ceria catalysts was analyzed using the H₂-TPR technique and the resultant H₂-TPR profiles are illustrated in **Fig. 3**. It is evident from the graph that with increase in copper loading, the reduction peaks for 5CC, 10CC, 15CC and 20CC shifts towards the lower temperature region. This judgement can be justified from the comparison of 5CC and 10CC catalysts suggesting that the metal support interaction decreases with increase in copper loading and is also suggestive of enhanced dispersion of copper species in the catalyst system³⁰. The 5CC catalyst showed two reduction peaks at 189 °C and 225 °C, which

correspond to the highly dispersed copper molecules in the

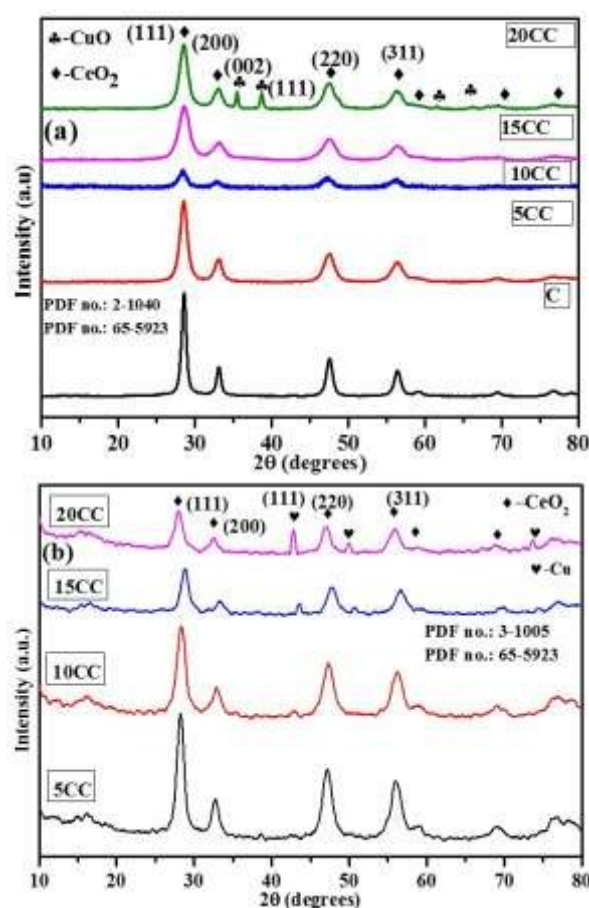


Fig. 2. XRD spectra of (a) calcined and (b) reduced CC catalysts.

ceria support matrix as well as the bulk copper molecules^{30, 31}. The other catalysts (10CC, 15CC) exhibit single peak at 198 °C and 209 °C, respectively which convinced us that the Cu²⁺

species is finely dispersed within the ceria support matrix. Further 20CC catalyst system shows the presence of shoulder peak at 184 °C along with a prominent peak at 205 °C which can be correlated with fine dispersion of Cu²⁺ species interacting strongly with ceria support at lower temperature and also due to bulkier copper molecules present on the CeO₂ support matrix³¹. It can also be observed that with the increase in copper loading, there is increase in the hydrogen consumption, suggesting that more amount of hydrogen utilisation for reduction delivers more availability of copper sites which possibly can enhance catalytic activity. The hydrogen consumption observed for 5CC, 10CC, 15CC and 20CC catalyst systems are 4.7, 7.6, 7.3 and 12.4 mmol g⁻¹, respectively. Thus, it can be concluded that this kind of dispersive behaviour combined with weak metal support interaction is responsible in governing the activity of these catalysts.

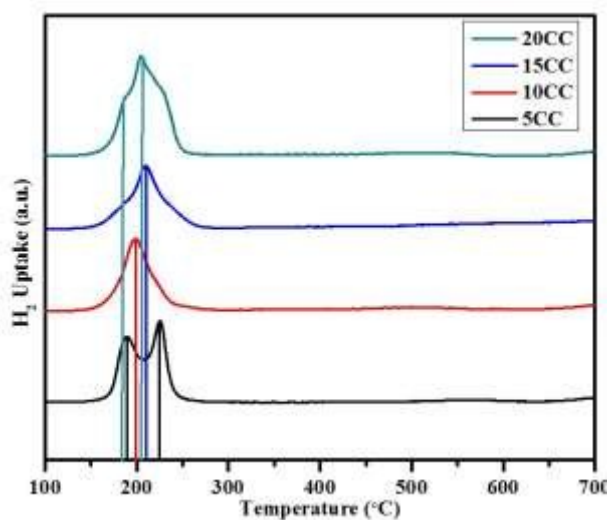


Fig.3. H₂-TPR profiles (a) 5CC, (b) 10CC, (c) 15CC, (d) 20CC catalysts.

N₂O Chemisorption studies: In order to determine extent of copper dispersion, copper metal surface area and its particle size, N₂O chemisorption analysis has been carried out and the respective results are tabulated in Table 1. As can be observed from the table, with gradual increase in the copper content, there is notable variation in surface properties of the catalysts. With increase in copper loading in 5CC, 10CC and 15CC catalysts, the metal surface area also increases. The metal surface area for 5CC, 10CC and 15CC catalysts show values as 30 m² g⁻¹, 56 m² g⁻¹ and 65 m² g⁻¹, respectively. With further increase in copper loading to 20 wt.% in 20CC catalyst, the surface area decreases to 32 m² g⁻¹. This decrease shows that when the amount of copper is greater than 15 wt.%, sintering takes place on the catalyst surface and hence the metal surface area in 20CC catalyst decreases. A general trend suggested that the dispersion of copper kept on decreasing with increase in copper loading. It can be observed that 5CC catalyst shows 90% dispersion whereas 10CC, 15CC and 20CC catalysts exhibit 86%, 67% and 25% dispersion, respectively.

This observation reasons out a clear indication for the absence of copper peaks in the XRD analysis upto 15wt.% addition of copper in the ceria support matrix. Additionally, it can also be inferred that high dispersion is possibly due to weak metal support interaction of copper with ceria support matrix. Moreover, metal particle size also influences the rate of dispersion. Hence, from the tabulated data it can be evidently seen that with the increase in addition of copper over ceria support matrix, the copper particle size increases.

The increase in metal particle size decreases the dispersion of metal onto the support matrix and similar trend is observed for all the aforementioned catalysts. 5CC catalyst exhibits smaller copper particle size with 1.11 nm whereas 10CC catalyst shows a moderate particle size with 1.21 nm. With further increase in copper loading to 15 wt.% and 20 wt.% in 15CC and 20CC catalysts, the particle size is seen to be 1.55 nm and 4.15 nm. The increase in the metal particle size with increase in copper loading can be due to the agglomeration of copper particles taking place on the support matrix which resultantly decreases the dispersion of copper species on the support matrix.

NH₃ & CO₂ temperature programmed desorption studies: The reaction pathway for dehydrogenation reaction can be governed by both acidic and basic properties of supported metal catalysts³². NH₃ and CO₂-TPD analysis was carried out to find the presence of acidic and basic sites along with the nature of available adsorption sites on the surface of (5, 10, 15, and 20CC) catalyst systems. The obtained TPD profiles are illustrated in Fig. 4. In NH₃-TPD, the basic NH₃ molecule adsorbs on the acidic centers of catalyst surface, whereas in CO₂-TPD a slightly acidic CO₂ adsorbs on the basic regions of the catalytic system. The variation in the desorption temperature is directly proportional to variation in acidity and basicity of the catalyst surface³³. Based on previous literature, the prominence of acidity and basicity can be interpreted based on the desorption peaks occurring at <300 °C, 300 °C-500 °C and 500 °C. These peaks are attributed to weak, intermediate and strong sites respectively^{24, 34}. In continuation, the NH₃-TPD profiles as shown in Fig. 4(a), displays the presence of NH₃ desorption peaks at lower than 300 °C suggesting that acidic sites in the catalyst system are present towards lower acidic region. Also, increase in copper loading displays increase in desorption temperature which explains that the number of acidic sites increase with the increase in copper loading (5CC-179 °C, 10CC, 15CC, 20CC-187 °C) on ceria support. Additionally, the amount of NH₃ consumed for 5CC, 10CC, 15CC and 20CC catalysts is 3.66 mmol g⁻¹, 2.49 mmol g⁻¹, 2.53 mmol g⁻¹ and 2.61 mmol g⁻¹, respectively. The obtained results from NH₃-TPD analysis indicate that copper addition strongly influences the strength of surface acidic sites.

Interestingly, it can be observed that catalysts also contain surface basic sites as depicted in Fig. 4(b). The CO₂-TPD profile for 5CC catalyst system display the existence of all three weak (192 °C), moderate (427 °C) and strong (635 °C) basic sites. With further increase in copper loading to 10 wt.%, 15 wt.% and 20 wt.% in 10CC, 15 CC and 20 CC catalyst, the CO₂

desorption temperature increases which is a clear indication of increase in basicity as seen in the respective graphs.

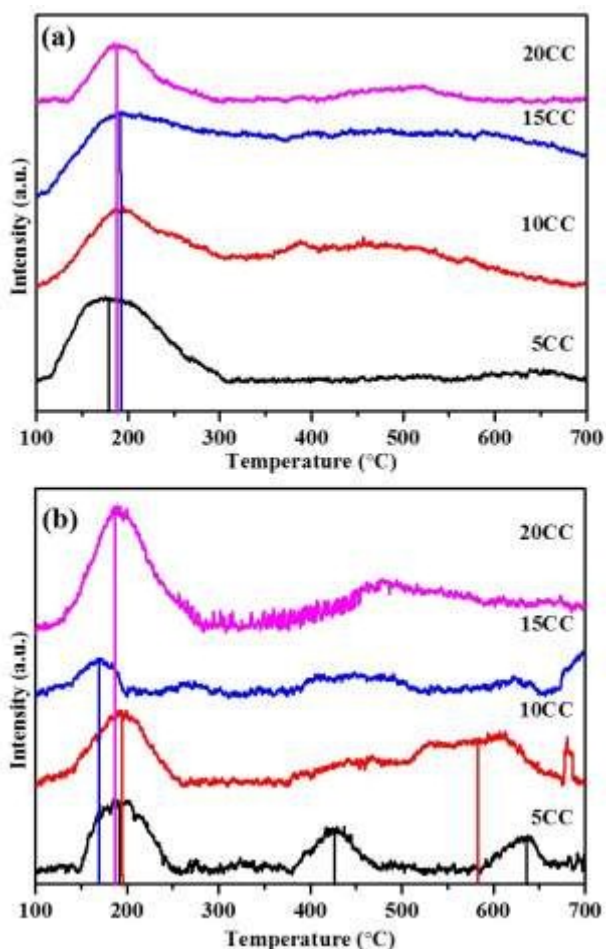


Fig. 4. (a) NH_3 and (b) CO_2 TPD profiles of CC catalysts with different metal loadings.

Interestingly, 10CC catalyst system shows the presence of weak ($194\text{ }^\circ\text{C}$) and strong ($583\text{ }^\circ\text{C}$) basic sites. Furthermore, prominent strong basic sites can be associated with (111) facets of CuO crystal phase of CC catalysts³⁵. In addition the amount of CO_2 consumed by 5CC, 10CC, 15CC and 20CC catalysts is 1.24 mmol g^{-1} , 1.53 mmol g^{-1} , 0.49 mmol g^{-1} and 1.61 mmol g^{-1} , respectively. Hence, based on literature reports and the results obtained from CO_2 -TPD, it can be said that these basic sites play a prime role in selective formation of GBL whereas the acidic sites favour the formation of THF as products.^{5,10} This also gives a probable explanation on the formation of slight amount of THF during the course of reaction as a by-product. The presence of strong basic sites majorly allows the synthesis of GBL as the prime product. As a concluding remark, the above mentioned NH_3 and CO_2 -TPD profiles of 5, 10, 15 and 20CC catalysts are indicative of occurrence of amphoteric character of all the as-synthesized catalyst systems.

ATR-IR analysis: In an attempt to determine the types of acidic as well as basic sites, pyridine and isopropanol adsorbed ATR-

IR spectra was recorded respectively and the consequent spectrograms are shown in Fig. 5. Pyridine being a basic molecule reacts with the acidic sites. The spectra have been recorded in the range of $1200\text{--}1800\text{ cm}^{-1}$. As shown in Fig. 5(a), with the increase in copper content in the as-synthesized catalyst systems (5, 10, 15 and 20CC), there is not much shift in the bands observed. The peak around 1437 cm^{-1} and 1583 cm^{-1} corresponds to the ring vibrations arising from the co-ordination of pyridine with Lewis acidic copper sites. Lewis acid sites combined with Bronsted acid sites can also be observed at 1484 cm^{-1} which is due to the co-ordination of pyridinium ions with these sites. There is not much variation in the intensities of peaks suggesting that the increase in copper content does not alter the acidic sites. Also, the spectra is suggestive of dual type of sites present in copper based ceria catalyst system^{22, 36, 37}.

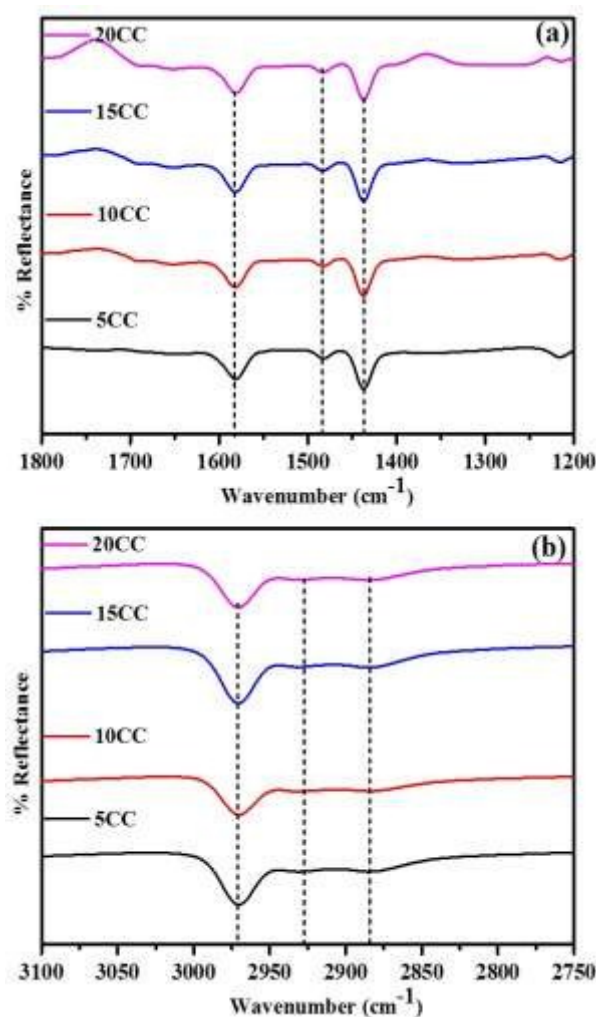


Fig. 5. ATR-IR spectra of CC catalyst (a) Pyridine adsorbed (b) IPA adsorbed probe molecules.

The nature and type of basic sites were determined using isopropanol (IPA) probed ATR-IR spectra and the results are displayed in Fig. 5 (b). The basic sites in the catalyst system interact co-ordinatively with the acidic protons of C-H groups in the IPA molecule. The spectrum was recorded in the band

region of 2750-3100 cm^{-1} . The relationship between basic sites and IPA can be determined by the change in frequencies related to symmetric stretching of C-H and CH_3 groups along with asymmetric stretching of CH_3 groups after the interaction of IPA with the catalyst surface. There is negligible change in the vibration frequencies of all the four catalysts with variation in addition of copper molecules. However, there is deviation with respect to asymmetric stretching of CH_3 groups. The 20CC catalyst system showed red shift (2968 cm^{-1}) whereas 5CC, 10CC and 15CC catalysts exhibit blue shift in the asymmetric region (2972 cm^{-1}). 5CC and 10CC catalysts also show blue shift (2930 cm^{-1}) towards the symmetric stretching of CH_3 group, whereas 15CC and 20CC catalysts exhibit red shift (2931 cm^{-1}) in this region. This is due to the interaction of CH_3 proton with the basic site on the catalyst surface. There is however no change in the symmetric stretching frequency of C-H groups of IPA for all catalyst systems observed due to co-ordinative interaction of acidic C-H proton with the basic site of the catalyst³⁸. With the increase in the copper loading there is increase in intensities of asymmetric stretching peaks related to CH_3 group which is suggestive of the influence of copper group in varying the basicity of catalysts. Hence, the above explained interpretations convey that the overall synergistic effect of Lewis basic as well as acidic sites is clearly depicted in the catalyst systems.

with copper loading of 10 wt.% is represented in Fig. 6, which exhibits the surface morphology of the as-synthesized fresh 10CC catalyst. As can be inferred from Fig. 6(a-c), the FE-SEM micrograph of fresh 10CC exhibits dispersed spherical morphology, which is a characteristic feature of copper and ceria based materials³⁹. The average particle size is calculated to be between 15 to 17 nm as shown in Fig. 6(d). The elemental composition of the 10CC catalyst is determined by EDX and mapping and the obtained results are displayed in Fig. 6(e) and Fig. 6(f), respectively. From the figure, it can be clearly observed that only O (9.63%), Ce (80.15%) and Cu (8.41%) elements are detected in 10CC fresh catalyst with no other elements. This proves that copper particles are finely dispersed on the surface of the ceria support matrix.

TEM Analysis: A thorough examination was executed using TEM and HR-TEM analysis for exploring the microstructural architecture of the 10CC catalyst as shown in Fig. 7(a-d). It was seen that the 10CC catalyst possesses spherical morphology which is a characteristic silhouette exhibited by copper based ceria materials.⁴⁰ Additionally, this observation is well-supported and in accordance with the results obtained from FE-SEM analysis. Fig. 7(e) displays a typical high resolution TEM image of the 10CC catalyst. The average particle size based on HR-TEM analysis was calculated to be in the range of 7 nm. This observation confirms the highly crystalline nature of the 10CC catalyst. The Lattice fringes with a d-spacing of 0.35

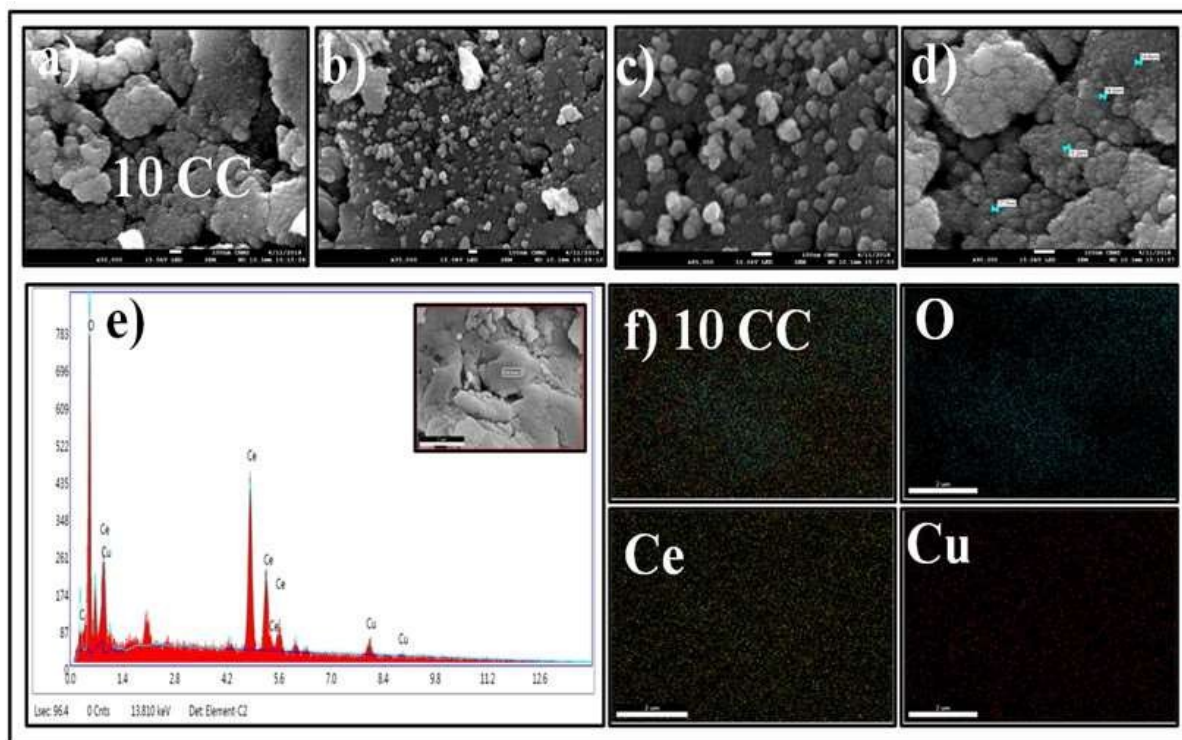


Fig. 6(a-d). FE-SEM micrographs, (e) EDX analysis and (f) mapping of 10CC fresh catalyst.

FE-SEM Analysis: The activity studies carried out with 10 wt.% copper based ceria catalyst showed better results hence, the FE-SEM analysis was carried out for 10CC catalyst. The morphological characteristics of copper based ceria catalysts

nm was observed which corresponds to the (111) crystallographic plane of ceria in the 10CC catalyst. Moreover, the black patches seen in the TEM images (Fig. 7(a,b)) correspond to the presence of Cu in the 10CC catalyst. The EDS

analysis was performed to confirm this observation. As can be clearly seen from **Fig. 7(g)** that 10CC catalyst comprises of Cu element along with Ce and O elements. **Fig. 7(f)** displays SAED pattern of the as-synthesized 10CC catalyst which confirms its polycrystalline nature. This observation also provides secondary support to the XRD results. The planes corresponding to (111), (220) and (200) were observed for the concentric rings in 10CC catalyst⁴¹.

Catalytic activity study:

Effect of temperature and Cu loading on the catalytic activity:

After the successful characterization of the as-synthesized catalysts, they were tested for their respective catalytic behaviours. To begin with, dehydrogenation of 1,4-BDO was carried out in vapour phase medium at various temperatures viz. 240, 260, 280, 300 °C using 5CC, 10CC, 15CC, 20CC copper based ceria catalysts. The major products obtained on

conversion of 1,4-BDO were GBL and tetrahydrofuran (THF). The effect of temperature on the catalytic activity of copper based ceria catalysts for their respective conversion and selectivity and the graphical representation is shown in **Fig. 8(a)** and **Fig. 8(b)**, respectively.

Fig. 8(a) shows that with gradual increase in temperature there is a steady decrease in the conversion of all the synthesized catalysts (5CC, 10CC, 15CC, 20CC). This observation can be attributed to the carbon deposition or agglomeration of copper particles in the CC catalysts⁵. Consequently, their selectivity towards GBL formation tends to decrease with increase in temperature (**Fig. 8 (b)**). This can be attributed to the increase in the number of acidic sites in due course of reaction at higher temperatures, which favours formation of by-product (THF). With further increase in temperature, less amount of 1,4-BDO gets converted which can be related to agglomeration of copper particles occurring

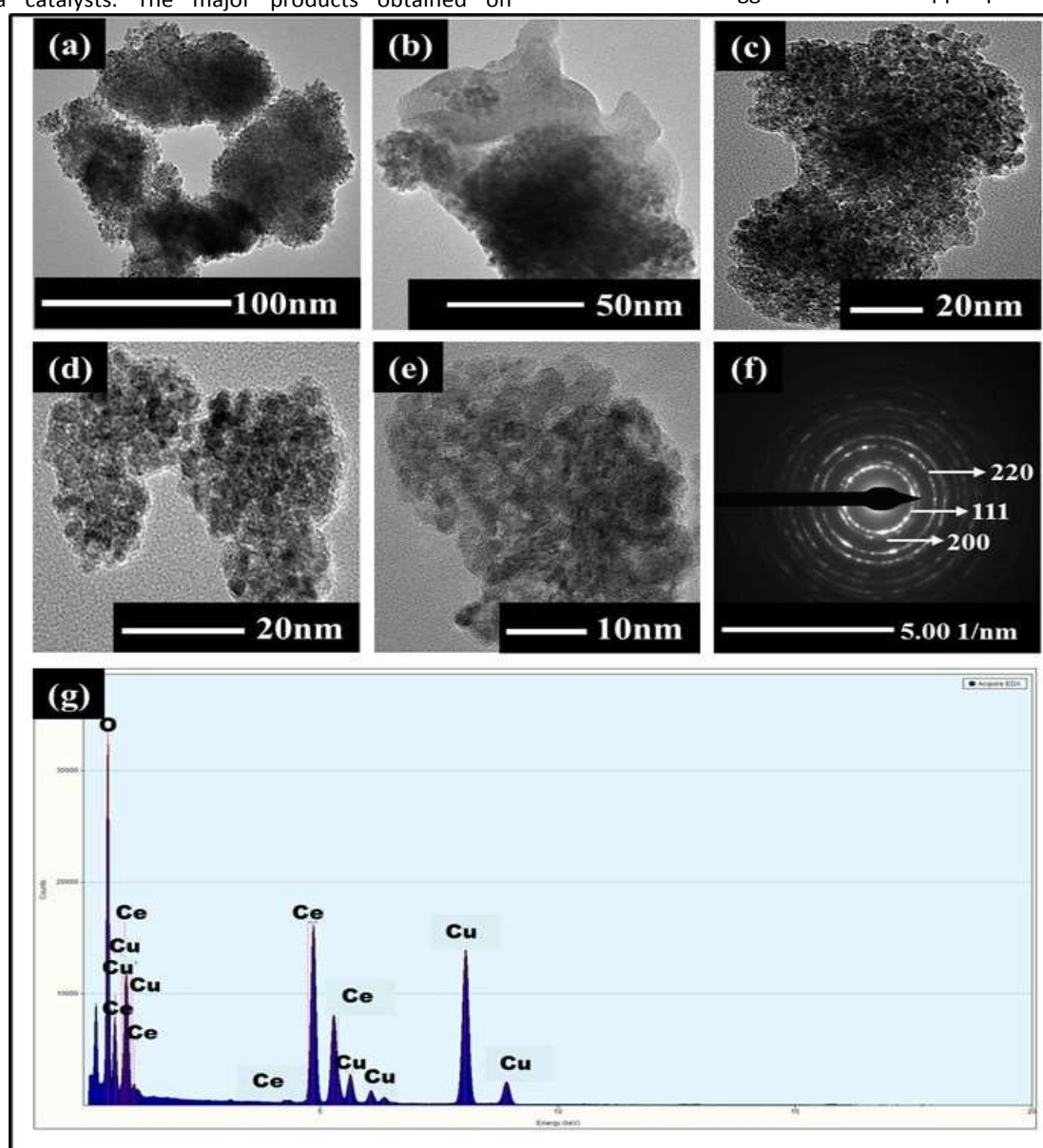


Fig. 7(a-d) TEM images of 10wt.% Cu/CeO₂ catalyst, **(e)** HR-TEM image of 10wt.% Cu/CeO₂ catalyst, **(f)** SAED pattern of 10wt.% Cu/CeO₂ catalyst and **(g)** EDS of 10wt.% Cu/CeO₂ catalyst.

at higher temperatures. As a result, surface availability of active sites decreases on which the reactant adsorbs which indirectly prevents the conversion. Subsequently, deposition of carbon from cracking of the reactant molecule may occur at higher temperatures. Considering the above conditions, 240 °C is regarded as the optimum temperature for carrying out further studies. The effect of copper loading on the activity of CC catalysts has also been investigated and the obtained results are listed in **Table 2**. Literature studies reported that merely support materials are inactive towards selective dehydrogenation of 1,4-BDO^{42, 43}. Additionally, on carrying out the reaction with bare ceria support, it revealed that bare supports show less conversion of 1,4-BDO with around 4% and selectivity towards GBL around 39%. In order to increase the activity of support, different metals have been used. In this regard, different amounts of copper loading: 5CC, 10CC, 15CC and 20CC were duly synthesized, characterized and tested for their catalytic activity towards the dehydrogenation of 1,4-BDO to GBL.

From **Table 2**, it is notable that with the increase in copper loading from 5wt.% (5CC) catalyst to 10wt.% (10CC) catalyst, conversion of 1,4-BDO increases (35% to 93%). With further increase in the copper loading to 15wt.% (15CC) catalyst, the conversion decreases to 87% which remains same for 20CC catalyst (**Fig. 8**). The selectivity of GBL shows similar trend and resemblance in its behaviour with all the four catalyst systems wherein the increase in copper loading invariably increases the

selectivity of GBL. The TOF values observed for the catalysts are represented in **Table 2**. The TOF values observed for 5CC, 10CC, 15CC and 20CC catalysts are 3092 $\mu\text{mol sec}^{-1} \text{site}^{-1}$, 4299 $\mu\text{mol sec}^{-1} \text{site}^{-1}$, 3442 $\mu\text{mol sec}^{-1} \text{site}^{-1}$ and 6838 $\mu\text{mol sec}^{-1} \text{site}^{-1}$, respectively.

This demonstrates that addition of copper metal to the catalyst system plays an effective role in governing the activity of catalysts. Interestingly, 10CC showed prominent results among all the other catalysts. The increase in the catalytic activity of 10CC can be attributed to its high surface area and metal support interaction. Additionally, physicochemical properties like fine dispersion of the 10CC catalyst as observed from XRD, TPR, N₂O chemisorption and SEM data, contributes immensely towards its higher activity. Furthermore, the presence of weak and strong basic sites as confirmed from CO₂-TPD, favours the selective formation of GBL when compared to acidic sites which favours THF formation. For higher loadings of copper catalysts (15CC and 20CC), we believe that sintering of copper particles lowers down their respective catalytic activity towards the production of GBL. Secondly, on comparing the surface area of 5CC, 10CC, 15CC and 20CC catalysts, it was found that 5, 15 and 20CC catalysts show a steep drop in catalytic activity which might be a result of the lesser surface area, which provides less area for adsorption of reactant molecules. Thus, considering the data towards catalytic activity, 10CC catalyst at 240 °C shows better catalytic activity and is regarded as the optimum catalyst to carry out further studies.

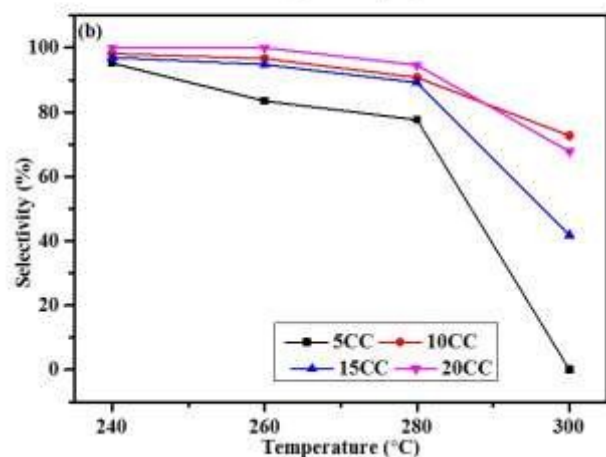
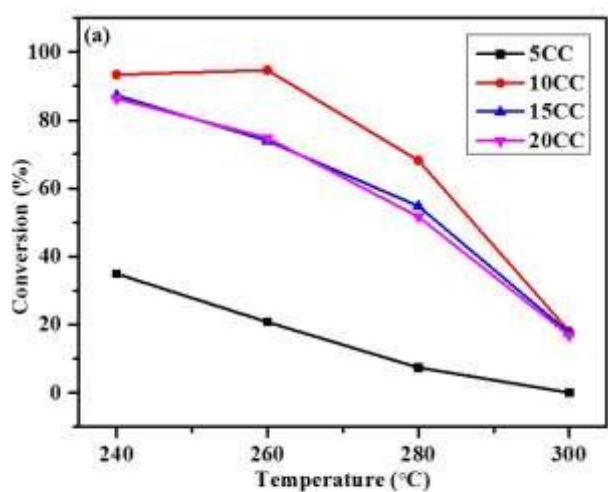
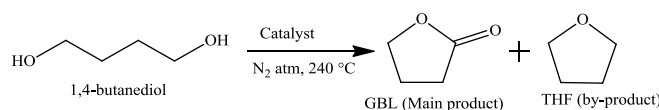


Fig. 8. (a) Effect of temperature with different copper loadings on ceria for the conversion of 1,4-BDO for 1 h reaction, (b) Effect of temperature with different copper loadings of ceria catalysts towards selectivity of GBL after 1 h. Reaction conditions: 0.5 g catalyst, 1 mL h⁻¹ 1,4-BDO feed and 30CC min⁻¹.

Table 2. Activity of catalysts with different Cu loadings, various supports for dehydrogenation of 1,4-BDO to GBL at 240 °C for 1h of reaction.



Sr. No	Catalyst	Conv. (%)	GBL Sel. (%)	THF Sel. (%)	Yield (%)	TOF ($\mu\text{mol}/\text{sec}/\text{site}$)
1	CeO ₂	4	39	61	2	-
2	5CC	35	95	5	33	3092
3	10CC	93	98	2	92	4299
4	15CC	87	97	3	85	3442
5	20CC	86	100	0	86	6838
6	10CuTi	3	0	100	0	-
7	10CuZn	14	48	52	7	-
8	10CuSBA-15	30	70	30	21	-
9	10CuAl	100	27	73	27	-
10	10CuZSM-5	100	9	91	9	-

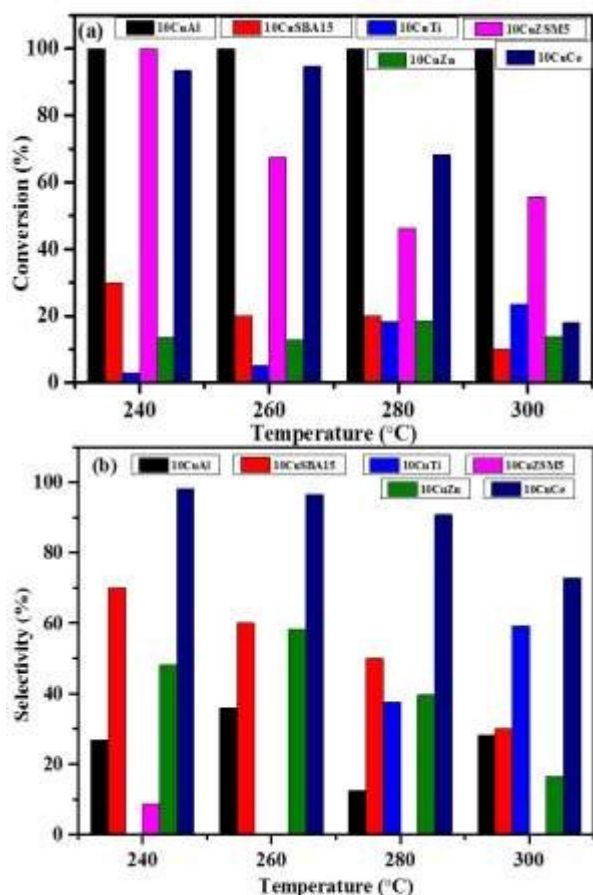


Fig. 9. Effect of temperature with different supports on 10wt.% of Cu for dehydrogenation reaction. **(a)** Conversion of 1,4-BDO and **(b)** Selectivity of GBL. Reaction conditions: 0.5 g catalyst, 1 mL h⁻¹ 1,4-BDO feed and 30CC min⁻¹ N₂ gas flow.

Effect of supports on the catalytic activity of 10 wt.% copper catalysts: The effect of various supports on the catalytic activity of 10wt.% copper catalysts is illustrated graphically in Fig. 9. It can be clearly observed that supports like Al₂O₃ and ZSM-5 show 100% conversion at all temperature whereas, supports like TiO₂, ZnO show much lower conversions due to their physicochemical properties. Interestingly, the selectivity towards GBL shown by these supports is comparatively low, owing to high acidic nature of these materials. In order to determine and confirm the acidic nature of the catalysts with various supports, NH₃ and CO₂-TPD analysis was carried out and the results are graphically represented in Fig. 10. Fig. 10(a) represents the NH₃-TPD data and Fig. 10(b) represents CO₂-TPD data of the catalysts with 10 wt.% Cu supported on Al₂O₃ (10CuAl), SBA15 (10CuSBA15), HZSM5 (10CuHZSM5), TiO₂ (10CuTi) and ZnO (10CuZn), respectively. From the NH₃-TPD profile it can be clearly observed that 10CuAl, 10CuSBA15, 10CuHZSM5, 10CuTi and 10CuZn catalysts exhibit all three types of acidic sites including weak, moderate and strong sites. The respective CO₂-TPD profiles of the above mentioned catalyst as shown in Fig. 10(b), confirms that there are basic sites. However, the comparison of both NH₃ and CO₂-TPD denotes that the amount of acidic sites are more compared to the basic sites and as a result the catalysts appear acidic in nature. This observation is accountable for the low selectivity of GBL from the dehydrogenation of 1,4-BDO using various supports.

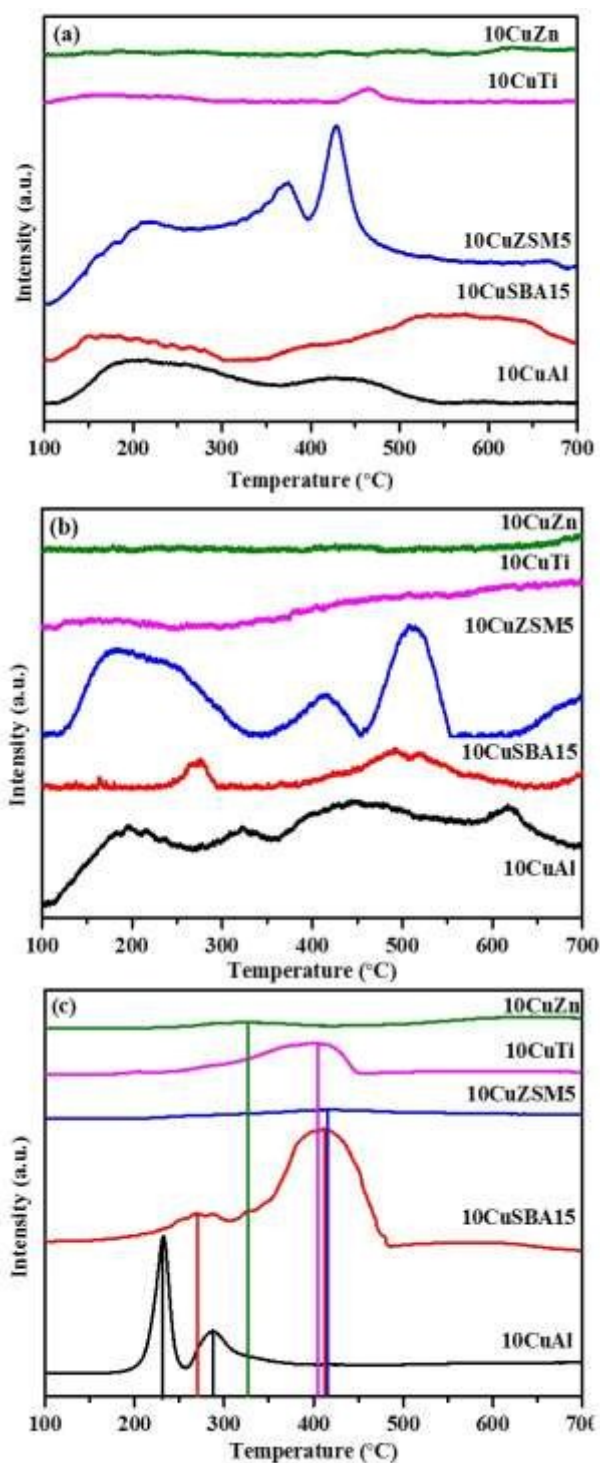


Fig. 10. (a) NH_3 -TPD, (b) CO_2 TPD and (c) H_2 -TPR profiles of 10wt.% Cu catalysts with different supports.

Secondly, extent of metal-support interaction, dispersion of copper on the support matrix was determined by H_2 -TPR and the results are displayed in Fig. 10(c). It can be clearly observed that the reduction temperature observed for all the catalysts is higher than the reduction temperature of Cu in CC catalysts. Thus confirming that 10 wt.% Cu catalysts with different support have low dispersion of Cu on the supports. With various factors mentioned above which

govern the catalytic activity 10 wt.% copper catalysts with supports like SBA-15, Al_2O_3 , TiO_2 and ZnO may have strong metal-support

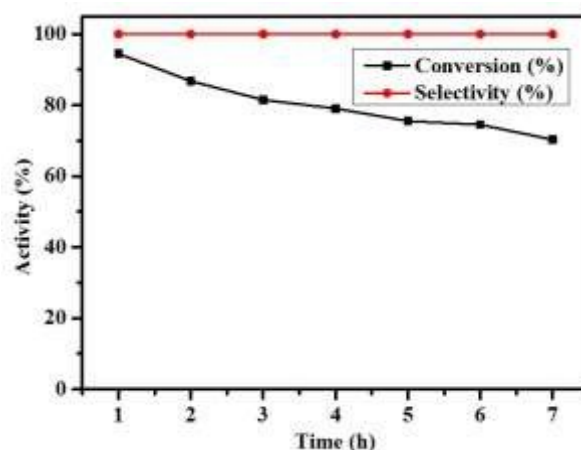


Fig. 11. The stability test for 10CC catalyst for the dehydrogenation of 1,4-BDO to GBL. Reaction conditions: 0.5 g catalyst, 1 mL h^{-1} 1,4-BDO feed, 240°C reaction temperature and 30CC min^{-1} N_2 gas flow.

interaction, high acidity, lower surface area, less dispersion of copper particles which may result in decrease in catalytic activity of

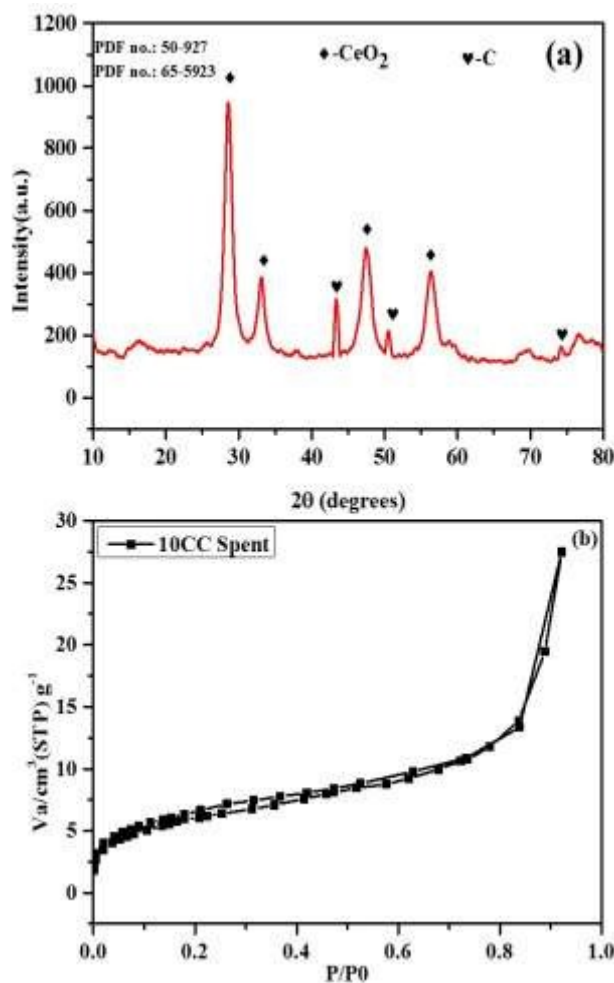


Fig. 12. (a) XRD Spectra of 10CC spent catalyst. (b) N_2 -physorption analysis of 10CC spent catalyst.

10 wt.% Cu catalysts with different supports. Aforementioned, considering all the facts 10CC is considered the best catalyst for dehydrogenative cyclisation of 1,4-BDO.

Time on stream studies: The elucidation of potential role of catalysts is studied using time on stream analysis for 10CC catalyst at 240 °C and the result is displayed in **Fig. 11**. Notably, with the passing time, conversion decreases from 93% to 70%. About 25% decrease in conversion is observed however, the selectivity (98%) remains same throughout the run. Consequently, the conversion observed after second hour decreases from 93% to 87% and similar trend is observed for consecutive hours. The decrease in conversion with time can be attributed to coke deposition on the catalyst surface and also sintering of copper particles which can be observed and confirmed from FE-SEM and EDX data. Additionally, XRD plot of the used catalyst shows the presence of carbon deposition in the rhombohedral phase (ICDD: 50-927) along with ceria (ICDD: 65-5923) at 2θ values 43.47°, 50.50°, 74.35° over the catalyst surface which is evident from **Fig. 12(a)**. N_2 physisorption analysis of spent catalyst is suggestive of decrease in surface ($24\text{m}^2/\text{g}$) area and the presence of a type II isotherm (**Fig. 12(b)**) which demonstrates that deposition of coke particles leads to decrease in porosity⁴⁴.

Secondly, in order to determine the surface morphology of 10CCU spent catalyst FE-SEM analysis was carried out and the resulting images are represented in **Fig. 13(a-d)**. In case of spent 10CCU catalyst, the spherical parental morphology is retained even after being used. It can be observed that the particles on the surface of the catalyst show agglomeration and there is simultaneous increase in the average particle size (15 to 20nm) (**Fig. 13(d)**). This can be

attributed to the coke deposition on its surface which can be confirmed from the EDX mapping of spent 10CCU catalyst. This also concludes that during the course of the reaction the agglomeration of the particles influence its catalytic activity. In case of 10CCU spent catalyst, O (3.77%), Ce (69.15%), Cu (7.95%) and C (3.77%) particles are present as can be observed from EDX analysis and mapping of spent catalyst in **Fig. 13(e-f)**. Also, carbon is the only element detected in the sample along with Ce, Cu and O in the 10CCU spent catalyst. The mapping analysis depicts that vapour phase reaction leads to the coke deposition on the surface of the catalyst which accounts for the presence of carbon in the 10CCU spent catalyst.

In order to explicate the formation of coke on the surface of 10CC catalyst system thermogravimetric analysis was carried out for spent 10CCU catalyst and the resultant thermogram is displayed in **Fig. 14(a)**. The thermogram clearly depicts deposition of coke on the surface of 10CCU catalyst at around 500 °C²⁴. The amount of coke deposited can be accounted to 4% which is similar to the results obtained in EDX analysis of spent catalyst. Initial drop in weight percentage at 50 °C in the thermogram may be due to expulsion of moisture present in the catalyst. The sole reason for the drop in catalytic activity can be related to coke deposition and we believe this may also be the reason why the catalysts shows agglomeration after the catalytic run.

Furthermore, TEM and HR-TEM analysis was performed to confirm the deposition of carbon on the 10CCU spent catalyst surface as displayed in **Fig. 14(b)**. It can be clearly observed that the characteristic spherical parent morphology of 10CC catalyst is well-

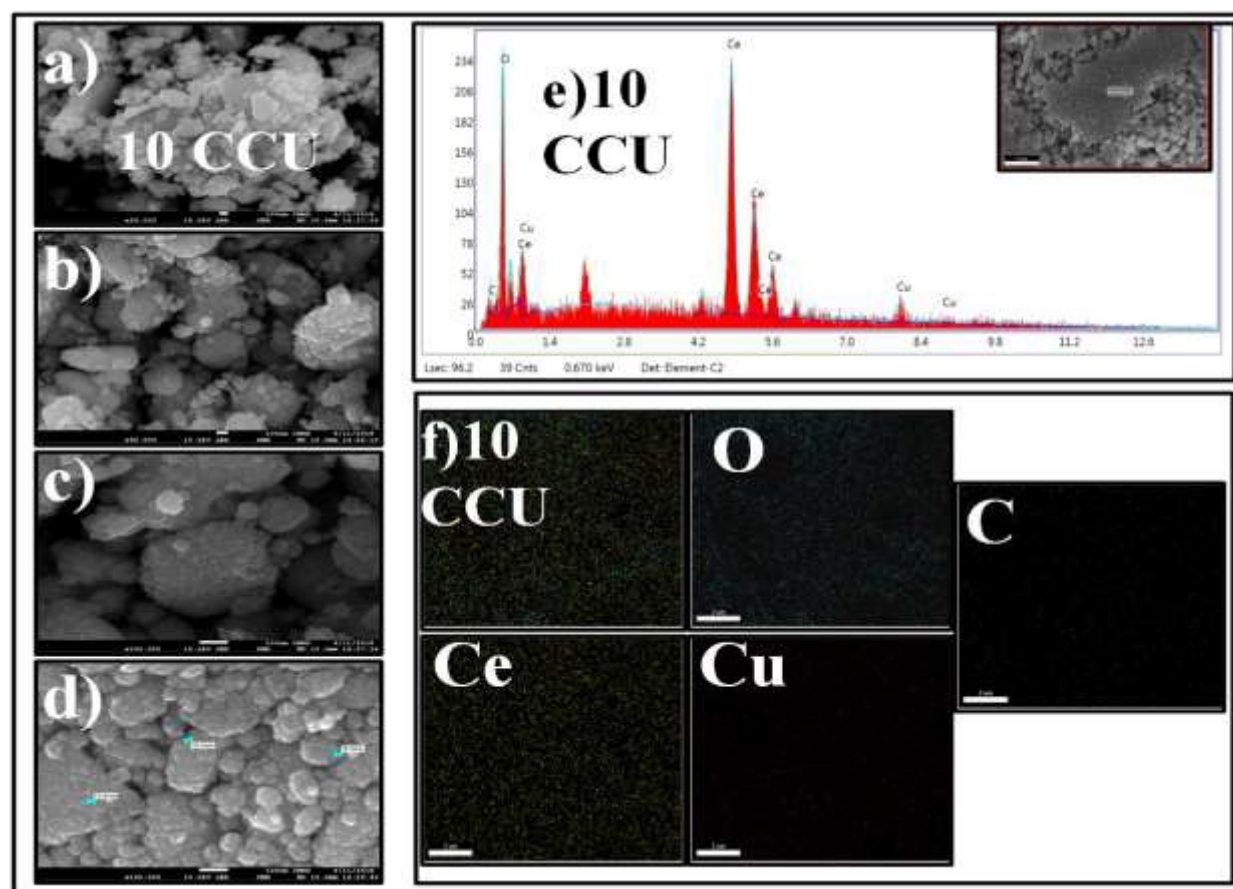


Fig. 13(a-d). FE-SEM micrographs, **(e,f)** EDX analysis and mapping of 10CCU spent catalyst.

preserved in the 10CCU spent catalyst. Notably, the images depict the clear visible agglomeration of the Cu particles in the 10CCU spent catalyst. Additionally, based on the HRTEM image carbon deposition could be clearly observed in the lattice fringes of the 10CCU spent catalyst. Further, the EDS analysis also shows the presence of carbon along with Cu, Ce and O. This observation further provides secondary support to the TGA analysis of the 10CCU spent catalyst which also conveys that there was deposition of carbon species on the 10CCU catalyst. The SAED pattern also shows that the polycrystalline nature of the 10CC catalyst is retained in the 10CCU spent catalyst.

Various researchers have elucidated the mechanistic pathway of dehydrogenation of 1,4-BDO. The mechanism over catalytic dehydrogenation of 1,4-BDO can be attributed as suggested by Zhang *et al.*², Ichikawa *et al.*³ and Huang *et al.*⁸. The plausible mechanistic pathway for oxidative catalytic dehydrogenation of 1,4-BDO is picturised in **Scheme 1**. As per the mechanism, the reaction follows two steps. In the first step 1,4-BDO undergoes

dehydrogenation over the copper surface to give 4-hydroxybutanal along with interaction of reactant molecule (1,4-BDO) with the 10CC catalyst surface. The proton gets abstracted from one of the hydroxyl groups by the basic sites of the 10CC catalyst. Secondly, the hydride ion transfer results in the formation of highly unstable 4-hydroxybutanal intermediate. The latter step involves hemiacetylation of 4-hydroxybutanal and finally undergoes dehydrogenation to give GBL as the product. The initial part of this step involves hemiacetylation of 4-hydroxybutanal to 2-hydroxytetrahydrofuran (2HTHF). Later, the basic sites of the 10CC catalyst as observed from CO₂-TPD analysis and ATR-IR spectroscopy abstracts the proton from the hydroxyl group to give an intermediate. However, the charge transfer between oxide ion of the intermediate and hydride ion transfer from the C-H group generates the final product GBL. Resultantly, the formed product (GBL) desorbs from the 10CC catalyst surface and closes the catalyst cycle.

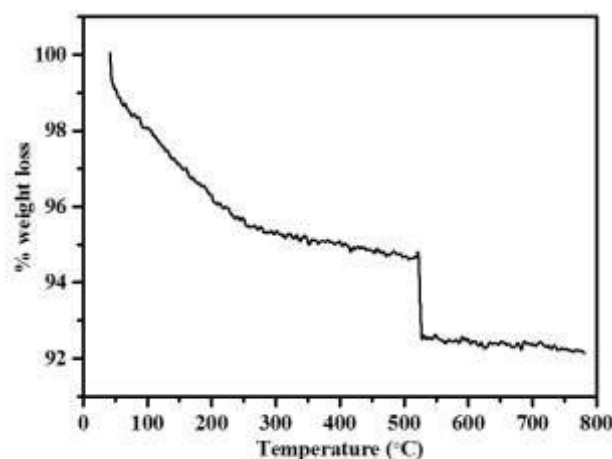


Fig. 14(a). Thermogravimetric analysis of 10CC spent catalyst used for dehydrogenation of 1,4-BDO to GBL.

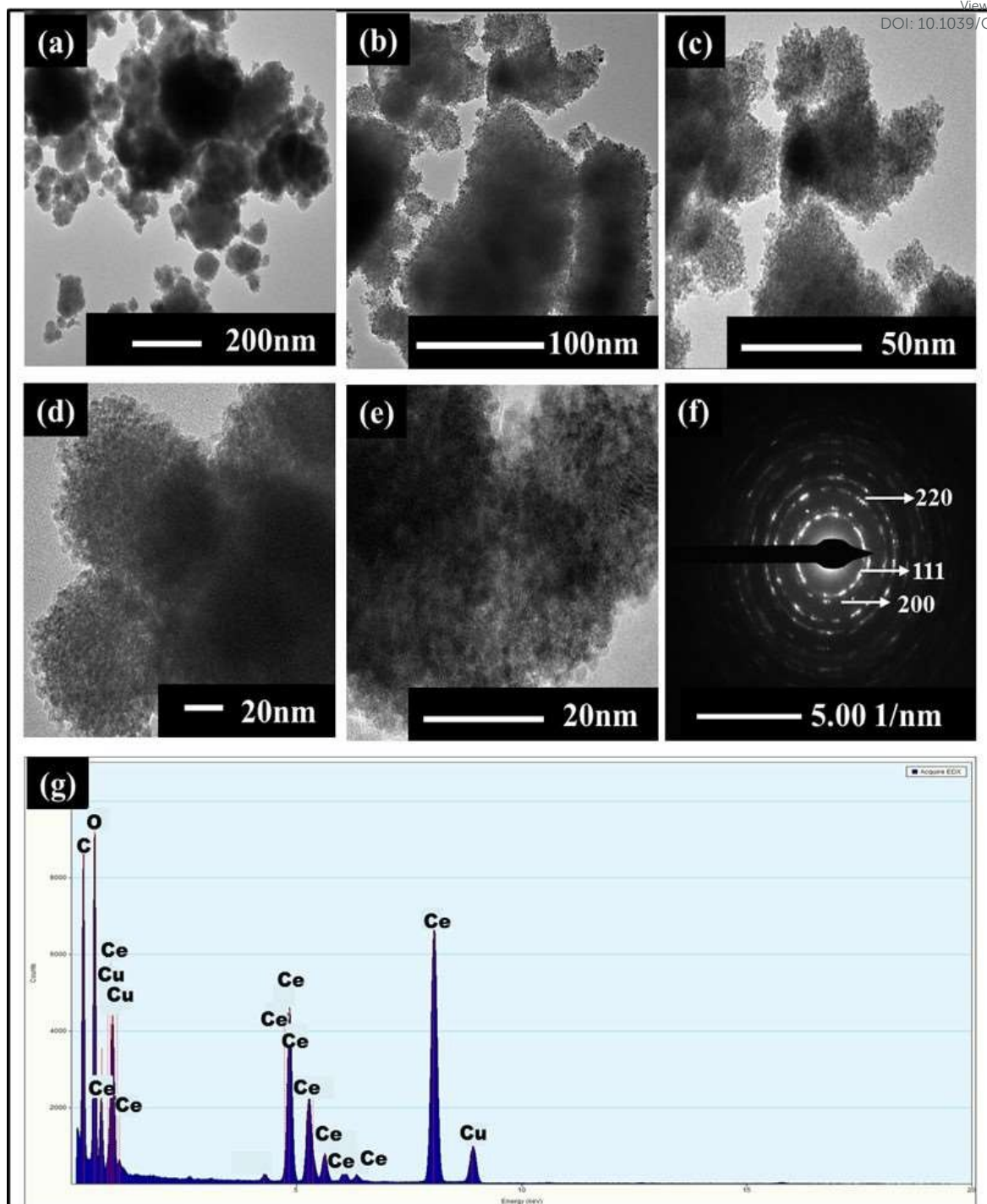
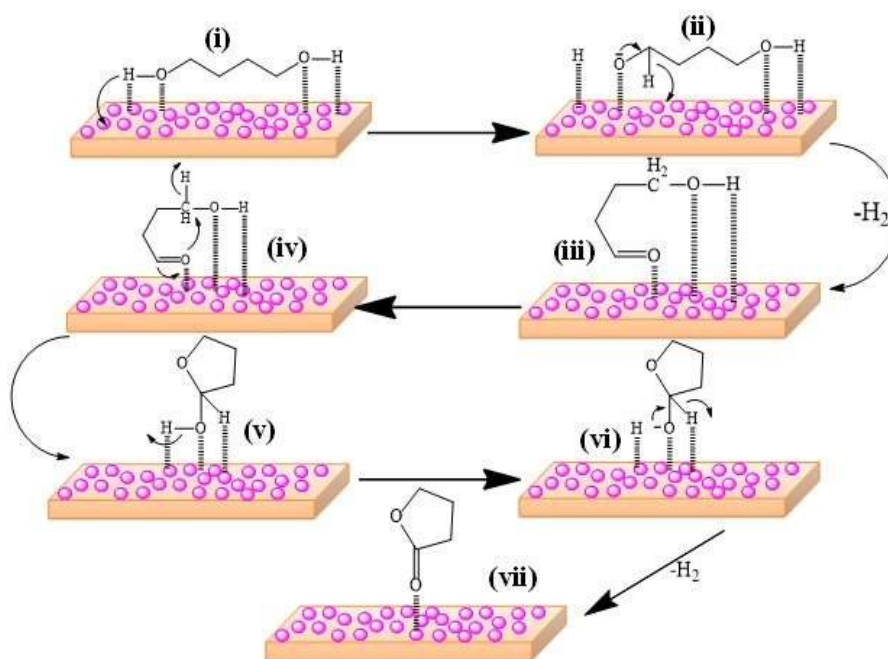


Fig. 14(b) TEM, HR-TEM, SAED pattern and EDS images of 10CCU spent catalyst.



Scheme 1. Plausible mechanism of dehydrogenation of 1,4-BDO to GBL over CC catalysts.

The comparison of various reported catalytic systems along with the present catalyst system towards dehydrogenation of 1,4-BDO has been summarised in **Table 3**. Reddy *et al.* reported the use of Cu-Co/MgO, Cu/MgO for dehydrogenation of 1,4-BDO along with the coupling reaction of 1,4-BDO with hydrogenation of various reactants at 250 °C and atmospheric pressure (**Table 3, Entries 1-5**). The reactions gave conversion ranging from 87% to 99% and selectivity ranging from 98-100%. Ichikawa *et al.* reported the use of Cu-ZnO-ZrO₂-Al₂O₃ for dehydrogenation of 1,4-BDO (**Table 3, Entry 6**). The reaction was carried out at 240 °C and atmospheric pressure in order to obtain a conversion of 84% and selectivity of 98%. Various authors tried dehydrogenation of 1,4-BDO with different catalysts in liquid phase medium. Huang *et al.* carried out liquid phase reaction of 1,4-BDO using Au/TiO₂ and Au/Fe₂O₃ at 140 °C, 1.25 MPa pressure (**Table 3, Entries 10-11**). The conversion obtained was 95-99% with 99-100% selectivity. Ichiki *et al.* reported the use of Cu-Cr-Mn in liquid phase dehydrogenation of 1,4-BDO at 230 °C and 0.4 MPa pressure (**Table 3, Entry 7**). The conversion obtained was 99% and selectivity was 97%. Various other catalysts were reported for dehydrogenation of 1,4-BDO at different temperature and pressures which showed good to low selectivity towards GBL formation (**Table 3, Entries 8-9, 12-14**). These already reported reactions either used promoters or were carried out at high temperatures. The present work was performed using Cu/CeO₂ catalysts at 240 °C at atmospheric pressure giving a conversion of 93% and selectivity of 98%. The key to obtain better selectivity towards the GBL is the presence of basic sites in the catalysts. The performance of the present work without the use of promoter and under low temperature condition proves the efficiency of the present catalyst system with the reported literature.

Conclusions

Copper based ceria catalytic systems were synthesized successfully by simple wet impregnation method. Selective vapour phase dehydrogenation of 1,4-BDO to GBL was carried out at various temperatures (240-300 °C) and different copper loadings (5, 10, 15 and 20 wt.%) using 5CC, 10CC, 15CC, 20CC catalysts and their influence on the catalytic activity was studied. Catalytic activity tests confirmed that 10CC catalyst was highly active at 240 °C for the selective dehydrogenation reaction with 93% conversion and 98% selectivity. The characterization studies confirmed that the cause for the better activity of the catalyst systems was attributed to their respective physicochemical properties. Namely, fine dispersion of copper metal onto the ceria support, greater surface area and basic nature of catalyst particles was responsible for better catalytic activity. Additionally, the effect of supports like TiO₂, ZnO, Al₂O₃, SBA-15, ZSM-5 on the catalytic activity of copper supported catalysts was also carried out and the results have been elucidated in detail. Further screening of all the synthesized catalysts along with a summarized comparison table of reported catalysts showed that the copper based ceria catalytic system exhibited the highest conversion and selectivity for the aforementioned reaction due to its highly basic nature. The stability test using time on stream analysis suggested that the catalyst activity was stable for 7 h with about 23% decrease in conversion, however, the selectivity remained same. The decrease in the activity of copper based ceria (10CC) catalyst was attributed to the coke deposition, sintering of copper particles and decrease in surface area.

Table 3. Comparison of different catalyst systems for

Sr. No.	Catalyst	Temp. (°C)	Press. (atm)	Conv. (%)	Sel. (%)	Ref.
1	Cu-Co/MgO	250	1	95	98	10
2	Cu/MgO	250	1	87	100	5
3	Cu-Co/MgO	250	1	95	96	45
4	Cu/MgO	250	1	96	99	46
5	Co-Cu/MgO	250	1	99	99	47
6	Cu-ZnO-ZrO ₂ -Al ₂ O ₃	240	1	84	98	3
7	Cu-Cr-Mn*	230	0.4	99	97	6
8	Cu/ZnO/Al ₂ O ₃	240	0.3	100	99	1
9	Cu-CaO-Na ₂ O/SiO ₂	210	1	100	98	7
10	Au/TiO ₂ *	140	1.25	99	100	8
11	Au/Fe ₂ O ₃ *	140	1.25	95	99	9
12	ZSM-5*	225	1.5	94	0	42
13	ZrO ₂	350	1	86	0	43
14	Cu-Ba/SiO ₂	240	1	99	100	2
15	Cu/CeO ₂	240	1	93	98	Present work

*:pressure in MPa

dehydrogenation of 1,4-BDO.

Conflicts of interest

The authors state that there are no conflicts to declare.

Acknowledgements

The authors thank Prof. Geetha R. Balakrishna, Director, CNMS, Jain University, Bangalore, India and Head of department, I & PC division, IICT, Hyderabad, India for their constant support. The authors thank Nano Mission, DST, Government of India, for financial support SR/NM/NS-20/2014.

References

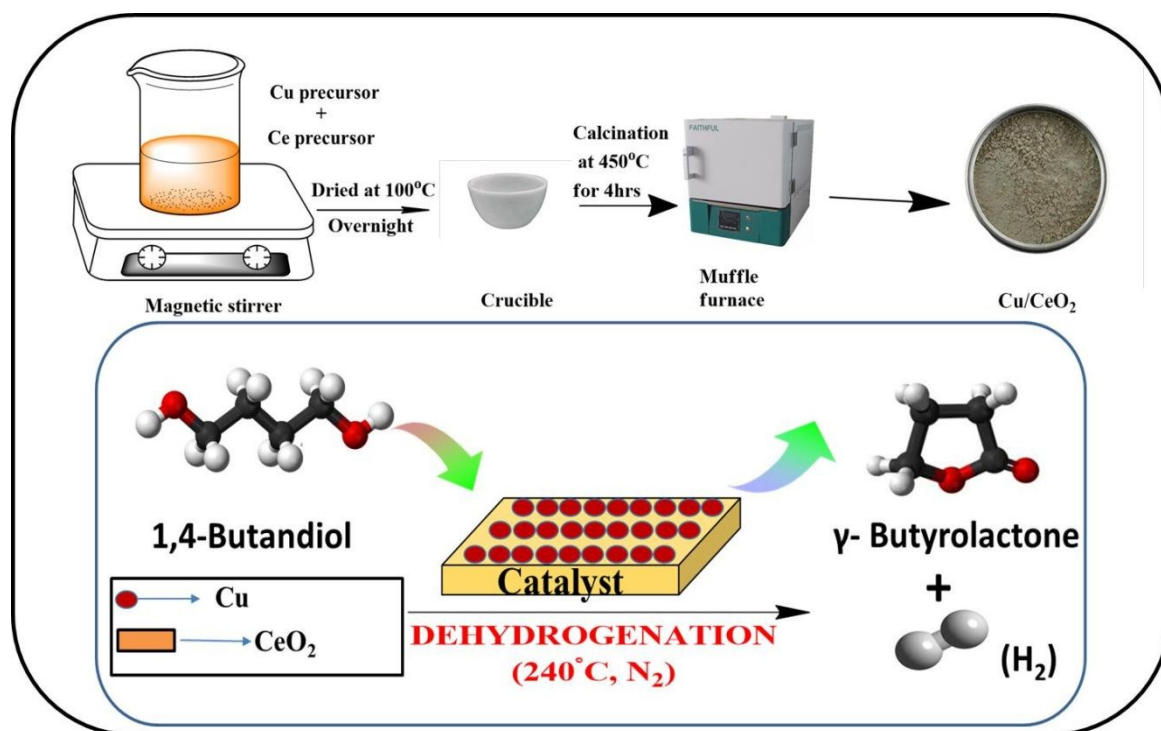
1. Y. L. Zhu, J. Yang, G. Q. Dong, H. Y. Zheng, H. H. Zhang, H. W. Xiang and Y. W. Li, *Applied Catalysis B: Environmental*, 2005, 57, 183-190.
2. B. Zhang, Y. Zhu, G. Ding, H. Zheng and Y. Li, *Applied Catalysis A: General*, 2012, 443-444, 191-201.
3. N. Ichikawa, S. Sato, R. Takahashi, T. Sodesawa and K. Inui, *Journal of Molecular Catalysis A: Chemical*, 2004, 212, 197-203.
4. D. W. Hwang, P. Kashinathan, J. M. Lee, J. H. Lee, U. H. Lee, J. S. Hwang, Y. K. Hwang and J. S. Chang, *Green Chemistry*, 2011, 13, 1672-1675.
5. K. Hariprasadreddy, R. Rahul, S. Sreevardhanreddy, B. Davidraju and K. Ramarao, *Catalysis Communications*, 2009, 10, 879-883.
6. K. M. T. Ichiki, S. Suzuki, H. Ueno and K. Kobayashi, US Patent No. 5210229, 1993.
7. H.J. Mercker, F. F. Pape, J. Simon, A. Henne, M. Hesse, U. Kohler, R. Dostalek, C. F. Erdbrugger and D. Kratz, US patent No. 6093677, 2000.
8. J. Huang, W. Dai, H. Li and K. Fan, *Journal of Catalysis*, 2007, 252, 69-76.
9. J. Huang, W. L. Dai and K. Fan, *Journal of Physical Chemistry C*, 2008, 112, 16110-16117.
10. K. H. P. Reddy, N. Anand, P. S. S. Prasad, K. S. R. Rao and B. D. Raju, *Catalysis Communications*, 2011, 12, 866-869.
11. M. Piumetti, S. Bensaid, N. Russo and D. Fino, *Applied Catalysis B: Environmental*, 2015, 165, 742-751.
12. Qi Fu, H. Saltsburg and M. F. Stephanopoulos, *Science*, 2003, 301, 935-938.
13. C. Tang, H. Zhang and L. Dong, *Catalysis Science & Technology*, 2016, 6, 1248-1264.
14. K. Tomishige, H. Yasuda, Y. Yoshida, M. Nurunnabi, B. Li and K. Kunimori, *Green Chemistry*, 2004, 6, 206-214.
15. R.X. Valenzuela, G. Bueno, A. Solbes, F. Sapiña, E. Martínez and V. C. Corberán, *Topics in Catalysis*, 2001, 15, 481-488.
16. N. Haddad, A. Saadi, A. Löfberg, R. N. Vannier, E. Bordes-Richard and C. Rabia, *Journal of Molecular Catalysis A: Chemical*, 2015, 396, 207-215.
17. H. Pan, M. Xu, Z. Li, S. Huang and C. He, *Chemosphere*, 2009, 76, 721-726.
18. C. D. Pina, E. Falletta and M. Rossi, *Journal of catalysis*, 2008, 260, 384-386.
19. J. N. Keuler, L. Lorenzen and S. Miachon, *Applied Catalysis A: General*, 2001, 218, 171-180.
20. T. B. Jayesh, K. Itika, G. V. Ramesh Babu, K. S. Rama Rao, R. S. Keri, A. H. Jadhav and B. M. Nagaraja, *Catalysis Communications*, 2018, 106, 73-77.
21. D. Zhao, J. Feng, Q. Huo, N. Melosh, G. H. Fredrickson, B. F. Chmelka and G. D. Stucky, *Science*, 1998, 279, 548-552.
22. S. S. Enumula, K. S. Koppadi, V. R. Babu Gurram, D. R. Burri and S. R. Rao Kamaraju, *Sustainable Energy & Fuels*, 2017, 1, 644-651.

23. I. Kainthla, G. V. Ramesh Babu, J. T. Bhanushali, R. S. Keri, K. S. Rama Rao and B. M. Nagaraja, *New Journal of Chemistry*, 2017, 41, 4173-4181.
24. I. Kainthla, G. V. R. Babu, J. T. Bhanushali, K. S. R. Rao and B. M. Nagaraja, *Journal of CO₂ Utilization*, 2017, 18, 309-317.
25. B. M. Nagaraja, C. H. Shin and K. D. Jung, *Applied Catalysis A: General*, 2013, 467, 211-223.
26. Y. Liu, K. Fang, J. Chen and Y. Sun, *Green Chem.*, 2007, 9, 611-615.
27. H. Zhu, Y. Chen, Z. Wang, W. Liu and L. Wang, *RSC Advances*, 2018, 8, 14888-14897.
28. T. B. Siregar and N. A. S. Amin, *Jurnal Teknologi*, 2006, 44(F), 69-82.
29. E. Shaaban, H. Hassan, S. Aly, H. A. Elshaikh and M. Mahmoud, *Applied Physica A*, 2016, 122, 722-730.
30. Z. Jiang, Z. Hao, J. Yu, H. Hou, C. Hu and J. Su, *Catalysis Letters*, 2005, 99, 157-163.
31. M. Lykaki, E. Pachatouridou, S. A. C. Carabineiro, E. Iliopoulou, C. Andriopoulou, N. Kallithrakas-Kontos, S. Boghosian and M. Konsolakis, *Applied Catalysis B: Environmental*, 2018, 230, 18-28.
32. H. P. R. Kannapu, Y.-W. Suh, A. Narani, V. Vaddeboina, D. R. Burri and R. R. Kamaraju Seetha, *RSC Advances*, 2017, 7, 35346-35356.
33. M. Lewandowski and Z. Sarbak, *Fuel*, 2000, 79, 487-495.
34. Z. Y. Zakaria, J. Linnekoski and N. A. S. Amin, *Chemical Engineering Journal*, 2012, 207-208, 803-813.
35. A. H. Jadhav, D. Prasad, H. S. Jadhav, B. M. Nagaraja and J. G. Seo, *Energy*, 2018, 160, 635-647.
36. S. S. Enumula, V. R. B. Gurram, R. R. Chada, D. R. Burri and S. R. R. Kamaraju, *Journal of Molecular Catalysis A: Chemical*, 2017, 426, 30-38.
37. Y. L. Yang and Y. Kou, *Chemical Communications*, 2004, 226-227.
38. T. Komanoya, K. Nakajima, M. Kitano and M. Hara, *The Journal of Physical Chemistry C*, 2015, 119, 26540-26546.
39. W. Liu, X. Liu, L. Feng, J. Guo, A. Xie, S. Wang, J. Zhang and Y. Yang, *Nanoscale*, 2014, 6, 10693-10700.
40. S. W. X. Zheng, X. Wang, S. Wang, X. Wang and S. Wu, *Materials Letters* 2005, 59, 2769-2773.
41. H. M. O. Amadine, K. Abdelouhadi, A. Fihri, S. El Kazzouli, C. Len, A. El Bouari and A. Solhy, *Journal of Molecular Catalysis A: Chemical*, 2014, 395, 409-419.
42. M. Aghaziarati, M. Kazemeini, M. Soltanieh and S. Sahebdehfar, *Industrial & Engineering Chemistry Research*, 2007, 46, 726-733.
43. A. Igarashi, S. Sato, R. Takahashi, T. Sodesawa and M. Kobune, *Catalysis Communications*, 2007, 8, 807-810.
44. I. Kainthla, V. R. B. Gurram, J. T. Bhanushali, S. R. R. Kamaraju, R. S. Keri, S. W. Gosavi, A. H. Jadhav and B. M. Nagaraja, *Catalysis Letters*, 2018, 148, 2891-2900.
45. H. P. R. Kannapu, Y.-W. Suh, A. Narani, D. R. Burri and R. R. Kamaraju Seetha, *Catalysis Letters*, 2016, 147, 90-101.
46. K. H. P. Reddy, Y.-W. Suh, N. Anand, B. D. Raju and K. S. R. Rao, *Catalysis Communications*, 2017, 95, 21-25.
47. H. P. R. Kannapu, C. K. P. Neeli, K. S. R. Rao, V. N. Kalevaru, A. Martin and D. R. Burri, *Catalysis Science & Technology*, 2016, 6, 5494-5503.

View Article Online
DOI: 10.1039/C9NJ03067K

Graphical Abstract

View Article Online
DOI: 10.1039/C9NJ03067K



Highlights

1. Copper based ceria catalysts were synthesized for dehydrogenation of 1,4-BDO to GBL.
2. Effect of supports on the catalytic activity of cu supported catalysts was also determined.
3. Copper based ceria catalysts exhibited conversion of 93% and 98% selectivity.
4. The catalysts showed stable activity upto 7 h with time.